metals

MDPI

Article

Effect of Tungsten Addition on Continuous Cooling Transformation and Precipitation Behavior of a High Titanium Microalloyed Steel

Zhenqiang Wang [1,*], Dongshen Huo [1], Yanyuan Zhou [1,*], Guoying Sui [1] and Fengchun Jiang [1,2]

[1] Key Laboratory of Superlight Materials and Surface Technology, Ministry of Education, College of Materials Science and Chemical Engineering, Harbin Engineering University, Harbin 150001, China
[2] Yantai Research Institute and Graduate School of Harbin Engineering University, Yantai 264006, China
* Correspondence: wangzhenqiang@hrbeu.edu.cn (Z.W.); zhouzyy123@hrbeu.edu.cn (Y.Z.)

Abstract: Effects of tungsten addition on the continuous cooling transformation (CCT) characteristics and precipitation behavior of a high titanium microalloyed steel were investigated by dilatometry, optical microscopy, scanning and transmission electron microscopy, and hardness measurements. The results showed that the ranges of transformation products were moved to the right side of the CCT diagram when the 0.4% W was added. Accordingly, the following observations were made: (i) the ferrite phase transformation was shifted to the side of lower cooling rates and reduced temperatures; (ii) the bainite phase transformation region ran throughout the whole cooling rate range studied. Addition of W had a positive effect on the particle size refinement and number density increase of the precipitates. At the low cooling rates, in the range of <14 °C/s, W addition shifted the precipitation hardening peak to the low cooling rate side as the ferrite transformation induced stronger precipitation strengthening than the bainite one. Furthermore, the effect of W addition on phase transformation strengthening was obvious (increase in hardness: ~40Hv) at the high cooling rate range, over 14 °C/s.

Keywords: transformation; precipitation; microstructure; hardness

check for updates

Citation: Wang, Z.; Huo, D.; Zhou, Y.; Sui, G.; Jiang, F. Effect of Tungsten Addition on Continuous Cooling Transformation and Precipitation Behavior of a High Titanium Microalloyed Steel. *Metals* **2022**, *12*, 1649. https://doi.org/10.3390/met12101649

Academic Editor: Beatriz López Soria

Received: 11 September 2022
Accepted: 27 September 2022
Published: 30 September 2022

Publisher's Note: MDPI stays neutral with regard to jurisdictional claims in published maps and institutional affiliations.

Copyright: © 2022 by the authors. Licensee MDPI, Basel, Switzerland. This article is an open access article distributed under the terms and conditions of the Creative Commons Attribution (CC BY) license (https://creativecommons.org/licenses/by/4.0/).

1. Introduction

The mechanical properties of low carbon steels are significantly enhanced through adding a small amount of microalloying elements (e.g., Nb, V and Ti) into them. Such types of steel are so called "microalloyed steels" [1]. Grain refinement and precipitation hardening are the two main factors that improve the strength of microalloyed steels. In recent years, more and more attention has been paid to steels with a titanium content of ≥0.1 wt.%, so called "high Ti-microalloyed steels", due to their lower production cost compared to Nb and V, and Ti microalloyed ones [2–21]. Mao et al. [2,3] successfully developed a high Ti-microalloyed steel with a yield strength of 700 MPa via compact strip production (CSP) technology. The microstructure of that steel is composed of fine ferrite and pearlite and dispersive nanoscale TiC particles. The increase in yield strength caused by precipitation hardening of TiC particles in this steel reached 120 MPa. For further improvement of the mechanical properties of high Ti-microalloyed steels, JFE corporation [11] produced a complex steel microalloyed with Ti and Mo, with the microstructure consisting of single-phase fine ferrite grains and dispersive complex nanoscale (TiMo)C particles. Such complex nanoscale carbides were found to possess superior coarsening resistance compared to pure TiC ones. The precipitation hardening effect from (TiMo)C carbides reached 300 MPa, which is 2–3 times higher compared to that of conventional microalloyed steels. Afterwards, a computational study showed [12] that similar to Mo, W could be incorporated into the TiC lattice to form complex (TiW)C particles with excellent coarsening resistance. Based on this idea, Park et al. [13] successfully developed a complex Ti-W

alloyed steel, in which the (TiW)C particles exerted significant precipitation hardening effect up to 350 MPa. However, compared to the role of W in the precipitation hardening, study on the phase transformation behavior of high Ti-microalloyed steels with W addition is still lacking.

The effect of W addition on the phase transformation characteristics and mechanical properties of steels has been studied extensively in previous research [22–25]. Totten et al. [22] examined the effect of W content on the isothermal phase transformation of carbon steels. They found that a high content of W in steel shifted the transformation regions to the longer-time range, as well as causing two separated transformation ranges in the diagram. Zhao et al. [23] examined the continuous cooling transformation (CCT) characteristics of Nb-V-Ti microalloyed steels with different W contents showing that W addition decreased critical cooling rates of phase transformations, induced a complete ferrite+pearlite microstructure formation and increased hardness. However, these studies did not involve the phase transformation that is accompanied by the significant precipitation of microalloying carbonitrides during the cooling process.

It is well known [2] that the significant amount of precipitation of microalloy carbides during or after $\gamma \rightarrow \alpha$ transformation is one of the typical characteristics of high Ti-microalloyed steels. In order to provide useful information for heat treatment and thermomechanical control process (TMCP) of high Ti-microalloyed steel, it is necessary to investigate the relationship between cooling process, phase transformation, and precipitation of microalloy carbide. Furthermore, for the most practical TMCPs, continuous cooling transformation data are needed [24]. Therefore, the aim of this study was to investigate the effect of W addition on the continuous cooling phase transformation and precipitation behavior of in high Ti-microalloyed steel, as well as to find the relationships among cooling process, transformation, and precipitation behavior.

2. Materials and Methods

The steels investigated in this paper were prepared by vacuum induction melting, and the chemical compositions of the as-cast steels were determined by optical emission spectrometry, as given in Table 1. An amount of 0.4 wt.% W was added to study the effect of W addition on the continuous cooling transformation (CCT) and precipitation behavior of Ti-microalloyed steel. The steels were prepared by vacuum smelting under Ar protective atmosphere, and then forged at 1100 °C to Φ26 mm bar. Homogenization at 1200 °C for 5 h was conducted followed by quenching. The thermal dilation tests were performed on Gleeble 1500D thermal simulator (DSI, St. Paul, MN, USA). The dimension of the specimen was Φ6 mm × 80 mm. The scheme of heating and cooling process is shown in Figure 1a. The heating temperature of 1200 °C was chosen as it was high enough to dissolve all the carbides except for a trace amount of TiN and $Ti_2S_2C_4$ particles [5]. The cooling rate (CR) varied from 0.27 °C/s to 30 °C/s. The dilation curves were recorded during a thermal cycle, as shown in Figure 1b. From Figure 1b, the Ac1 and Ac3 temperatures during the heating process, as well as the start and finish temperatures of phase transformation, T_s and T_f, were easy to detect. To characterize the microstructure after the thermal dilation test, the specimens were grounded, polished and etched by using 2% Nital solution. A metallographic microscope (OLYMPUS BX41M, OLYMPUS, Beijing, China) was utilized to observe the microstructures at different CRs. Microhardness was measured by a micro-Vickers sclerometer (HVS-1000A, HUAYIN, Laizhou, Shandong, China) with a load of 500 g and holding time of 15 s. The average hardness value was taken from five valid points.

Table 1. Chemical compositions of the investigated steels (wt.%).

Steel	C	Mn	Si	Ti	W	S	P	N
Ti	0.046	1.47	0.12	0.097	-	0.0060	0.0073	0.0024
Ti-W	0.041	1.50	0.20	0.095	0.39	0.0028	0.0060	0.0018

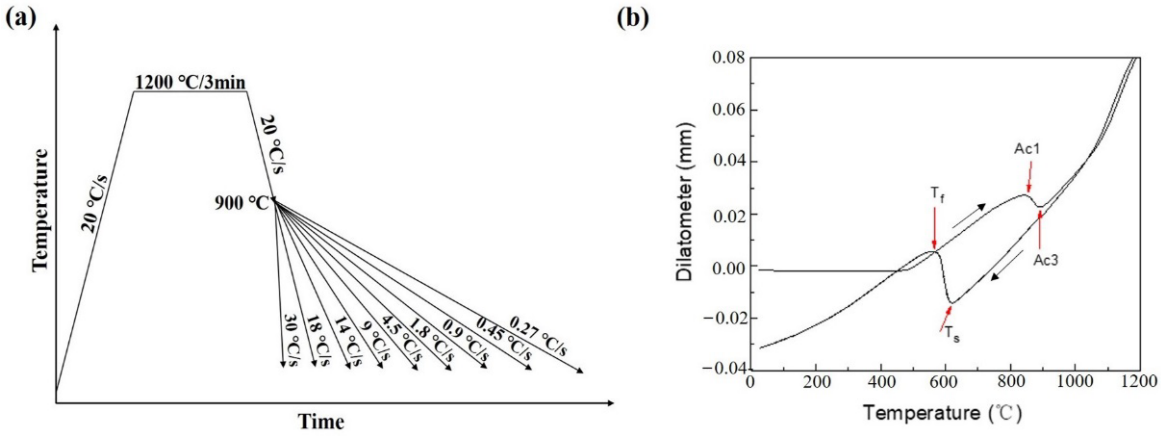


Figure 1. (**a**) Schematic diagram of the schedule for dilatometer tests and (**b**) dilatation versus temperature curve of Ti-W steel specimen at the cooling rate of 0.9 °C/s. Ac1 and Ac3 are austenization start and finish temperatures, respectively.

3. Results

3.1. CCT Diagram

Figure 2 shows the CCT diagrams for Ti and Ti-W alloyed steels where F denotes ferrite, B represents bainite, M_s and M_f are the start and finish temperatures of martensitic transformation, respectively. Since it is difficult to distinguish the finish temperature of bainite and start temperature of martensite on dilation curves, the Ms was calculated according to the following equation [26]:

$$Ms = 540 - 420[C] \quad (1)$$

$$[C] = C + \frac{Mn}{12} + \frac{Cr}{35} + \frac{Ni}{21} + \frac{Mo}{20} + \frac{W}{40} + \frac{Si}{40} - \frac{V}{3} - \frac{Al}{21} \quad (2)$$

where [C] is carbon equivalent, M (M = C, Mn, Cr, Ni, Mo, W, Si, V, and Al) is the wt.% of alloying elements in steel.

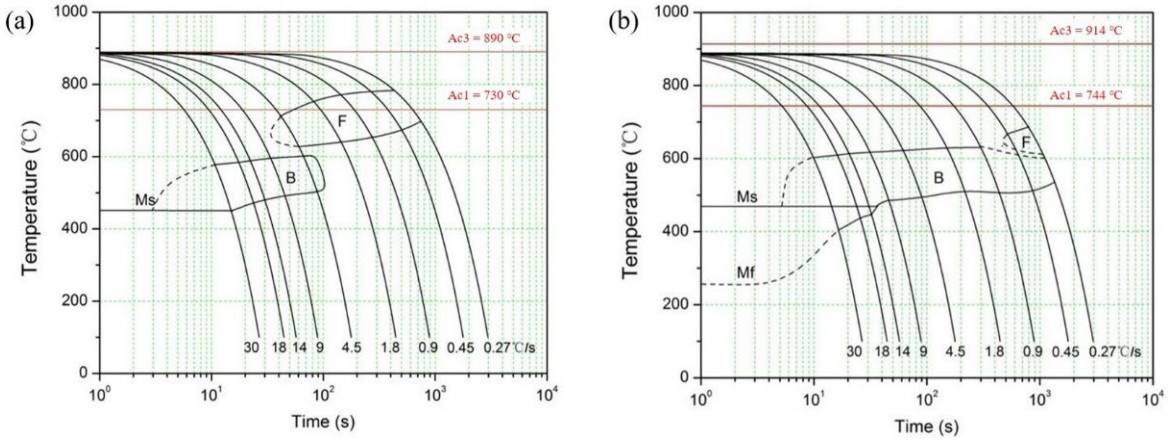


Figure 2. CCT diagrams of (**a**) Ti steel and (**b**) Ti-W steel. The dashed lines are the estimated ones.

It can be seen in Figure 2a that the microstructure of Ti steel was fully ferritic in the CR range of 0.27–1.8 °C/s. The start temperature of ferrite phase transformation ranged from 750 °C to 785 °C, and the finish temperature was between 640 °C and 695 °C. As the CR increased to 4.5 °C/s, the bainite phase transformation occurred, resulting in the formation of the ferrite-bainite microstructure. As the CR was further increased, a full bainite microstructure was obtained. By adding 0.4 wt.% of W, significant changes occurred

on the CCT diagram. First, the bainite phase transformation region ran throughout the whole studied CR range. The partially ferritic microstructure could be obtained in the CR range of 0.27–0.45 °C/s, whereas the ferrite phase transformation start temperature decreased to 660–670 °C. The fully bainitic microstructure was obtained in the CR range of 0.9–9.0 °C/s. Second, when the CR increased to 14 °C/s, the martensite phase transformation occurred after the bainite phase transformation. Moreover, it was clearly seen that W addition increased the austenization temperature. The measured Ac1 and Ac3 temperatures for Ti and Ti-W steels were: Ac1 = 730 °C and Ac3 = 890 °C for Ti steel; and Ac1 = 744 °C and Ac3 = 914 °C for Ti-W steel.

3.2. Microstructural Evolution

Figure 3 shows microstructures of continuously-cooled specimens at different CRs. The microstructure of Ti-microalloyed steel cooled with low CR, in the range of 0.27–0.9 °C/s, was fully ferritic. As the CR increased to 4.5 °C/s, the granular bainite microstructure appeared. With further increase of CR up to 14 °C/s, fully granular bainite microstructure was observed. When the CR reached 30 °C/s, formation of lath bainite started. For Ti-W alloyed steel, the microstructure composed of polygonal ferrite, granular bainite, and acicular ferrite mixture was observed for the CR of 0.27 °C/s. As CR rose to 0.9 °C/s, full granular bainite was observed. Further increasing CR up to 14 °C/s resulted in formation of the lath bainite and partial martensite microstructure. With increasing CR in this range, the volume fraction of martensite also increased (see Figure 3i). The microstructural observation indicated that addition of 0.4 wt.% W had significant impact on mictrostructural transformations during the continuous cooling process.

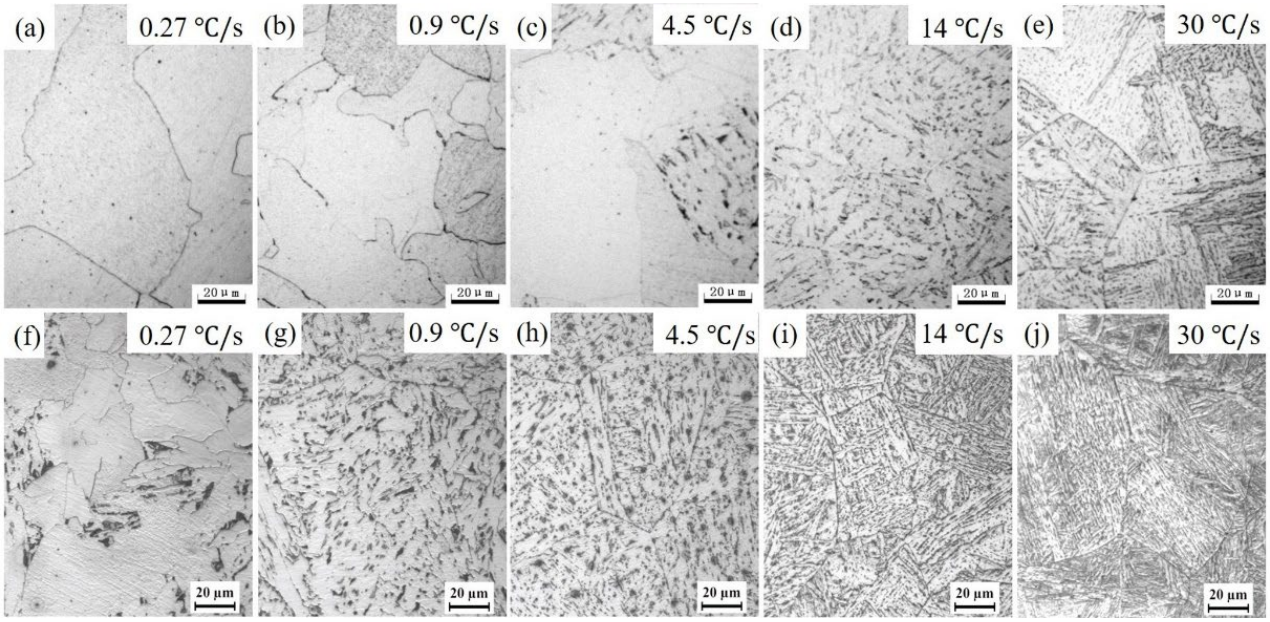


Figure 3. Optical microstructures of continuously-cooled specimens of (**a**–**e**) Ti steel and (**f**–**j**) Ti-W steel.

3.3. Hardness

The results of Vickers hardness of the continuously-cooled specimens at different CRs are shown in Figure 4. With the increase of CR, the hardness of Ti steel first increased sharply in the CR range of 0.27–4.5 °C/s, then decreased slightly, and, subsequently, there was a gradual increase as the CR became higher than 9 °C/s. For Ti-W steel, however, the Vickers hardness first decreased in the CR range of 0.27–0.9 °C/s and then increased gradually when the CR was over 0.9 °C/s. It is worth pointing out that, compared to Ti steel, Ti-W steel exhibited higher hardness values, except for samples cooled with CR of 4.5 °C/s, indicating the general strengthening effect caused by W addition.

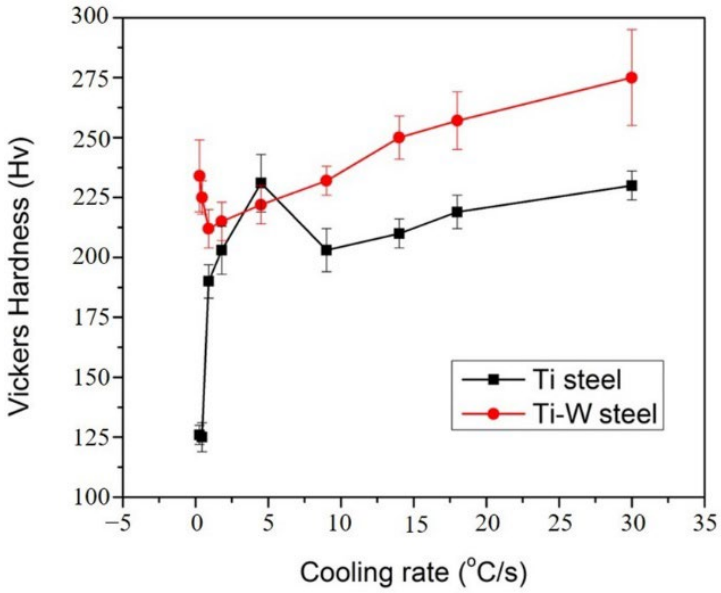


Figure 4. Dependence of hardness on cooling rate of the steels studied.

4. Discussion

4.1. Effect of W Addition on the Microstructural Evolution

As shown in Figures 2 and 3, W causes both quantitative and qualitative changes in the kinetics of transformation of the high titanium microalloyed steel. The results obtained by Zhao et al. [23] suggested that W shifts the transformation range to the longer-time range of the CCT diagram, which is consistent with our findings. The transformation ranges were shifted to the right side of the CCT diagram (see Figure 2), and the ferrite phase transformation temperatures decreased by addition of 0.4 wt.% W. As tungsten, which is the strong carbide-forming element, is added to the steel the carbon diffusion activation energy in austenite increases and, thus, its diffusion coefficient decreases and, hence, ferrite growth rate is lowered [27,28]. As a result, the formation of polygonal ferrite mainly dominated by carbon diffusion was limited due to W addition. Furthermore, W addition expanded the bainite phase transformation range, so that the bainite microstructure could be obtained at relatively low CRs, which was also consistent with the results of Zhao et al. [23]. Bainite transformation is a half-diffusion one and is dominated primarly by carbon diffusion [28]. Since W is a strong ferrite former [29], which can enhance the driving force of austenite to bainite phase transformation, it also increases the nucleation rate of bainite at a given temperature. Moreover, since the carbon diffusing speed is reduced, the growth of bainite is slowed down. Therefore, if some quantitative W is added to the steel, bainite transformation would occur in a wider temperature range, and as the growth rate decreases, the bainitic microstructure after transformation would be finer than that of W-free steel, as shown in Figure 3d,i.

4.2. Relationships among Cooling Process, Transformation and Precipitation and the Effects of W Addition

The hardness of the investigated steels is strongly related to both the type of microstructure and nanoscale precipitation [29]. For the steels which contain strong carbide formers, the CR not only influences the phase transformation but also affects the precipitation behavior of carbide during the cooling process. Based on the variations of microstructure (Figures 2 and 3) and microhardness (Figure 4), three specimens of Ti and Ti-W steel with different CRs were chosen for comparison, respectively. Figure 5 is the SEM image showing the distribution of precipitate particles in continuously-cooled Ti and Ti-W steels at three different CRs. The statistical particle size distributions of precipitates are shown in Figure 6. For Ti steel, at the low CR of 1.8 °C/s, the particle size was relatively large. As the CR

increased to 4.5 °C/s, at which a hardness peak was obtained (see Figure 4), the precipitates exhibited finer particle size with a higher number density. As the CR further increased up to 9 °C/s, only a few precipitates were observed, implying relatively weak precipitation hardening effect. These observations also explained why the hardness peak appeared at the CR of 4.5 °C/s. For Ti-W steel, the specimen with the CR of 0.27 °C/s had the largest number density of precipitates. With the increase in the CR, the density of precipitate decreased. At the CR of 14 °C/s, a very low number density of precipitates could be observed. As shown in Figure 3f, the microstructure at relatively low CR consisted of ~50% of ferrite. However, the precipitation hardening from precipitates was significant, leading to a higher hardness. At the CR of 0.9 °C/s, the granular bainite dominated the microstructure (Figure 3g), but the hardening from precipitation decreased due to the reduction of the density of precipitates within the matrix. With further increase in the CR to 14 °C/s, the precipitation hardening became very weak, whereas the lath bainite was formed (Figure 3i), leading to the gradual increase of hardness, due to the transformation strengthening effect. Furthermore, it should be noted that, compared to Ti steel, the precipitates in Ti-W steel were finer with higher number density, indicating that W addition had a positive effect on the refinement of the precipitates. Figure 7 shows the TEM analysis of the precipitates in Ti-W steel. The precipitates were identified as MC-type (FCC structure) carbide with a high content of W and a small amount of Ti and Fe. On the one hand, W addition decreased the temperature of $\gamma \rightarrow \alpha$ phase transformation (see Figure 2), as the addition of W possibly promoted the nucleation of precipitates by increasing the supersaturation of carbide formers and slowed down the growth of precipitates. On the other hand, it was noted [12] that the replacement of Ti by W in the MC lattice could decrease the interfacial energy by the reduction of strain energy at the interface, which had a beneficial retarding effect on the coarsening of the MC carbides. As a result, the sizes of precipitates were refined due to W addition.

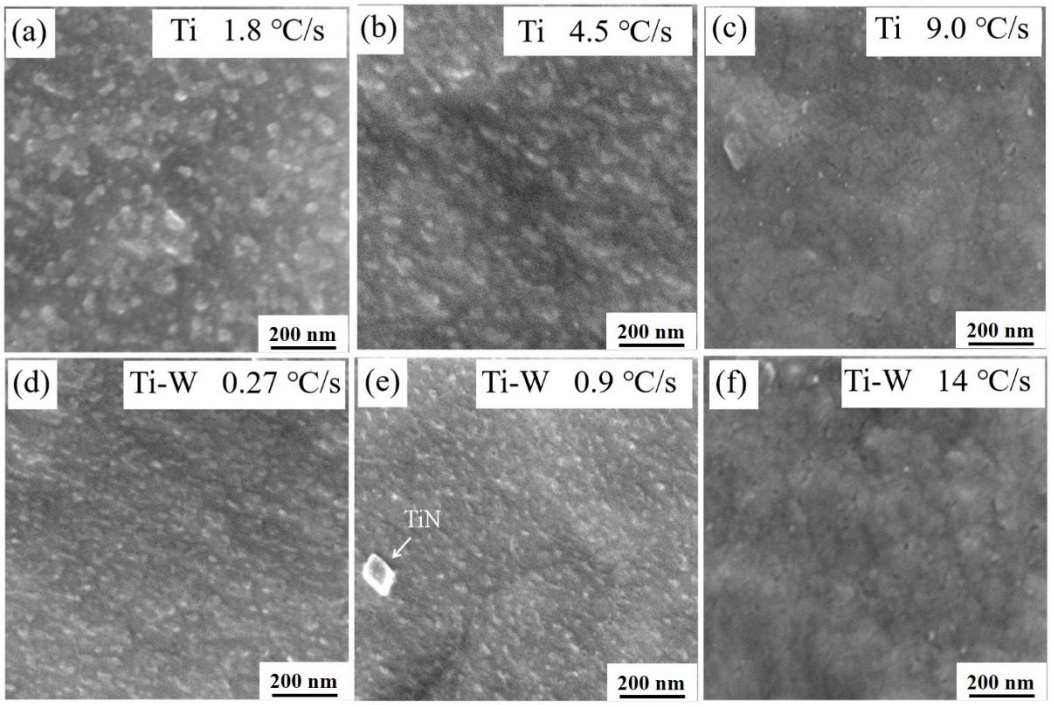


Figure 5. SEM image showing the precipitates in Ti and Ti-W continuously-cooled steel specimens. (**a**) Ti 1.8 °C/s, (**b**) Ti 4.5 °C/s, (**c**) Ti 9.0 °C/s, (**d**) Ti-W 0.27 °C/s, (**e**) Ti-W 0.9 °C/s, (**f**) Ti-W 14 °C/s.

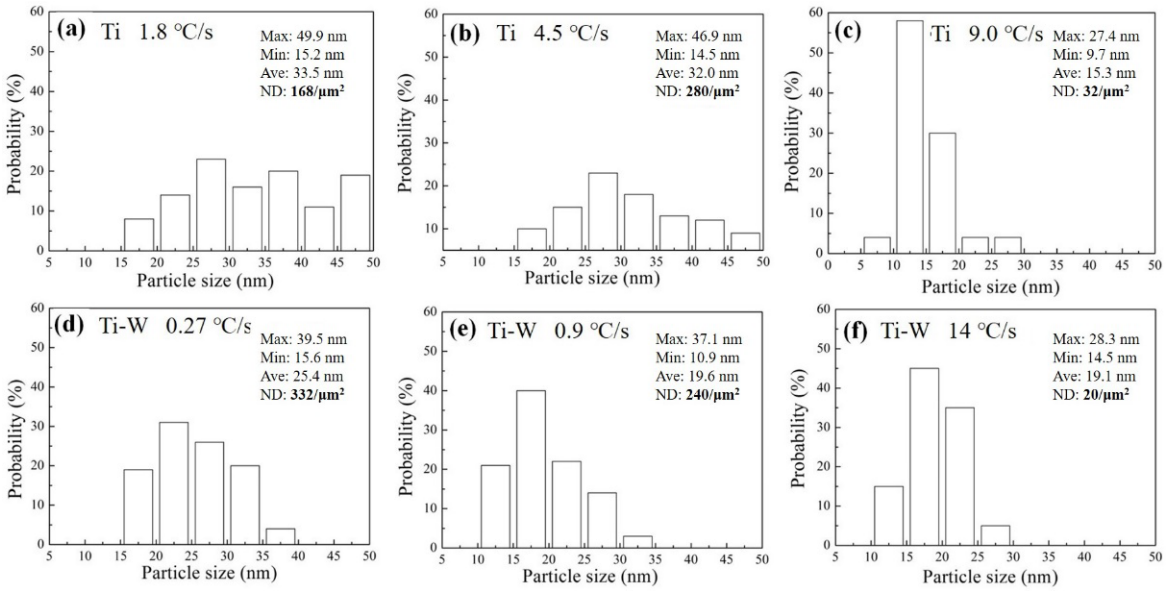


Figure 6. Particle size distribution of carbide precipitate in (**a**–**c**) Ti steel and (**d**–**f**) Ti-W steel. ND: number density per μm^2.

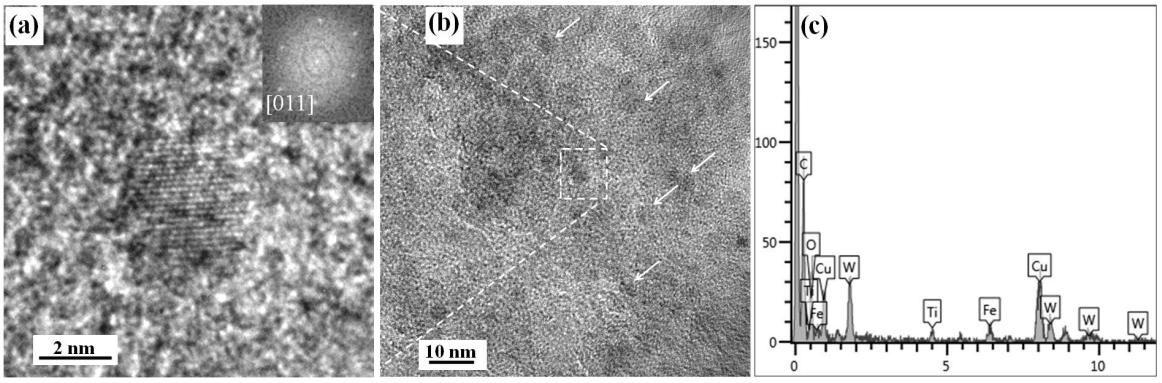


Figure 7. (**a**) HRTEM image and fast Fourier transformation (FFT) of the precipitate in (**b**), (**b**) TEM image showing the distribution of the nanoscale precipitates on carbon replica from Ti-W steel specimen obtained at the cooling rate of 0.9 °C/s, and (**c**) EDS analysis of the precipitate in (**a**). It should be noted that the FFT result in (**a**) indicates MC-type structure of the precipitate. The peaks of Cu and O in (**c**) are from the Cu grid which supported the replica film, and the inclusion in carbon replica film, respectively.

As shown in Figure 4, the CR at which maximum hardness was obtained, was 4.5 °C/s for Ti steel and 0.27 °C/s for Ti-W steel, corresponding with the critical CR of ferrite transformation. That is, W addition moved the precipitation hardening peak to lower cooling rates. In the ferrite transformation range, along with the increasing of CR, the precipitation hardening also increased. However, once the bainite transformation took place, the precipitation was highly inhibited, causing a sharp decrease in the hardness. For the continuous cooling process, which had negligible precipitation hardening effect, the relation between hardness and CR could be described by an empirical equation proposed by Wang et al. [30].

$$\mathrm{Hv} = \mathrm{a} + \mathrm{b} \times \exp(c \times v) + d \times \exp(e \times v) \quad (3)$$

where H_V is the Vickers hardness, v is the cooling rate, c, d and e are constants. For Ti-microalloyed steel, the precipitation hardening was impreceptile at very low CR, <0.45 °C/s. At CR higher than 14 °C/s, the precipitation hardening could also be ignored. For Ti-W steel, ignoring the solid solution strengthening effect from W due to

its relatively low content (0.4 wt.%), the hardness was considered to be the same as that of Ti steel at very low CR. As the CR was over 14 °C/s, the precipitation hardening in Ti-W steel also vanishes. The calculated relations between CR and hardness, as shown in Figure 7, were obtained by fitting to Equation (3). The chart in Figure 8 can be divided into two regions: precipitation hardening region at low CRs and non-precipitation hardening region at high CRs. For Ti steel, the hardness increased up to maximum of 70 Hv due to precipitation. For Ti-W steel, W addition shifted the hardness peak to the lower CR ranges, and the increase in hardness from precipitation reached ~100 Hv, which is higher than that of Ti steel. Furthermore, in the non-precipitation region, the transformation hardening effect due to W addition reached ~40 Hv, exhibiting significant strengthening effect.

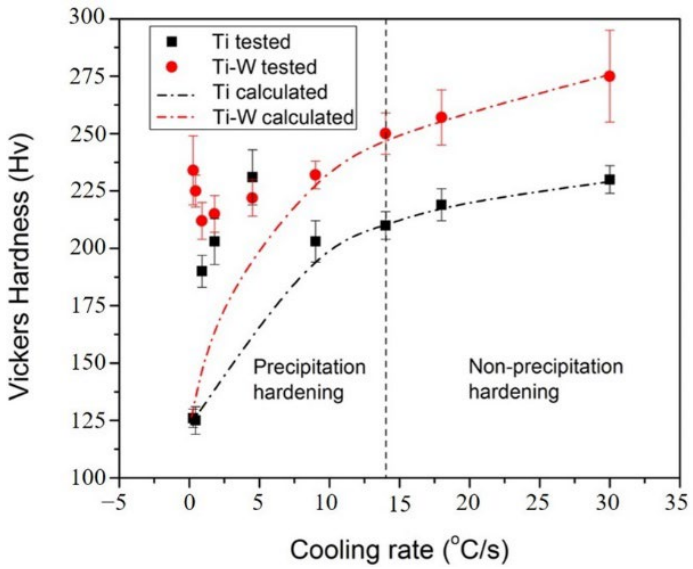


Figure 8. Comparison between the tested and calculated hardness values at different cooling rates.

5. Conclusions

CCT diagrams for high titanium microalloyed steel with and without W addition were determined, and the transformation characteristics and precipitation behavior during continuous cooling were studied. The following conclusions are drawn:

(1) W addition shifts the range of transformation products to the right side of the diagram. The ferrite transformation range moves to the side of lower cooling rates and reduced temperatures, and the bainite phase transformation range runs throughout the whole studied cooling rate range.

(2) W addition increases the ferrite to austenite transformation temperatures. The measured Ac1 and Ac3 temperatures for Ti and Ti-W steels are Ac1 = 730 °C and Ac3 = 890 °C for Ti steel; and Ac1 = 744 °C and Ac3 = 914 °C for Ti-W steel.

(3) W addition promotes the refinement of particle size and increases the number density of precipitates. The precipitates in Ti-W steel were identified as MC-type carbide with a high level of W and a small amount of Ti and Fe.

(4) In the precipitation hardening region, W addition moves the precipitation hardening peak to lower cooling rates, which is attributed to the shift of ferrite phase transformation to low cooling rates and reduced temperatures after W addition. In the non-precipitation region, W addition exerts significant transformation strengthening effect with the increase in hardness of 40 HV.

Author Contributions: Resources, funding acquisition, supervision, writing—review, Z.W.; formal analysis, data curation, writing—original draft preparation, D.H.; writing—original draft preparation, writing—review and editing, methodology, Y.Z.; investigation, G.S.; supervision, resources, F.J. All authors have read and agreed to the published version of the manuscript.

Funding: The authors appreciate the financial support by the National Natural Sciences Foundation of China (No. 52001084), the Tianjin Key Laboratory of Materials Laminating Fabrication and Interface Control Technology, the Jian-Hua Research Foundation of Hebei University of Technology (Nos. HB1921 and HB1920), and the Central University Foundation of Harbin Engineering University (No. GK2100260329).

Data Availability Statement: The data in this paper are obtained from experiments. All data generated in this study are included in this manuscript.

Conflicts of Interest: The authors declare no conflict of interest.

References

1. Yong, Q.L. *Microalloyed Steels-Physical and Mechanical Metallurgy*; Metallurgical Industry Press: Beijing, China, 1989.
2. Mao, X.P.; Huo, X.D.; Sun, X.J. Strengthening mechanisms of a new 700 MPa hot rolled Ti-microalloyed steel produced by compact strip production. *J. Mater. Proc. Technol.* **2010**, *210*, 1660–1666. [CrossRef]
3. Mao, X.P.; Sun, X.J.; Zhou, Y.L. Physical metallurgy for the titanium microalloyed strip produced by thin slab casting and rolling process. *Acta Metall. Sin.* **2006**, *42*, 1091–1095.
4. Xu, G.; Gan, X.L.; Ma, G.J. The development of Ti-alloyed high strength microalloy steel. *Mater. Des.* **2010**, *31*, 2891–2896. [CrossRef]
5. Wang, Z.Q.; Mao, X.P.; Yang, Z.G. Strain-induced precipitation in a Ti micro-alloyed HSLA steel. *Mater. Sci. Eng. A* **2011**, *529*, 459–467. [CrossRef]
6. Wang, Z.Q.; Yong, Q.L.; Sun, X.J. An analytical model for the kinetics of strain-induced precipitation in titanium micro-alloyed steels. *ISIJ Int.* **2012**, *52*, 1661–1669. [CrossRef]
7. Wang, Z.Q.; Sun, X.J.; Yang, Z.G. Effect of Mn concentration on the kinetics of strain induced precipitation in Ti microalloyed steels. *Mater. Sci. Eng. A* **2013**, *561*, 212–219. [CrossRef]
8. Tsai, S.P.; Su, T.C.; Yang, J.R. Effect of Cr and Al additions on the development of interphase-precipitated carbides strengthened dual-phase Ti-bearing steels. *Mater. Des.* **2017**, *119*, 319–325. [CrossRef]
9. Wang, T.P.; Kao, F.H.; Wang, S.H. Isothermal treatment influence on nanometer-size carbide precipitation of titanium-bearing low carbon steel. *Mater. Lett.* **2011**, *65*, 396–399. [CrossRef]
10. Huo, X.D.; Li, L.J.; Peng, Z.W. Effects of TMCP schedule on precipitation, microstructure and properties of Ti-Microalloyed high strength steel. *J. Iron Steel Res. Int.* **2016**, *23*, 593–601. [CrossRef]
11. Funakawa, Y.; Shiozaki, T.; Tomita, K. Development of high strength hot-rolled sheet steel consisting of ferrite and nanometer-sized carbides. *ISIJ Int.* **2004**, *44*, 1945–1951. [CrossRef]
12. Jang, J.H.; Lee, C.H.; Heo, Y.U. Stability of (Ti, M)C (M = Nb, V, Mo and W) carbide in steels using first-principles calculations. *Acta Mater.* **2012**, *60*, 208–217. [CrossRef]
13. Park, D.B.; Huh, M.Y.; Shim, J.H. Strengthening mechanism of hot rolled Ti and Nb microalloyed HSLA steels containing Mo and W with various coiling temperature. *Mater. Sci. Eng. A* **2013**, *560*, 528–534. [CrossRef]
14. Timokhina, I.; Miller, M.K.; Wang, J.T. On the Ti-Mo-Fe-C atomic clustering during interphase precipitation in the Ti-Mo steel studied by advanced microscopic techniques. *Mater. Des.* **2016**, *111*, 222–229. [CrossRef]
15. Zhang, K.; Yong, Q.L.; Sun, X.J. Effect of tempering temperature on microstructure and mechanical properties of high Ti microalloyed directly quenched high strength steel. *Acta Metall. Sin.* **2014**, *50*, 913–920.
16. Zhang, K.; Li, Z.D.; Wang, Z.Q. Precipitation behavior and mechanical properties of hot-rolled high strength Ti-Mo-bearing sheet steel: The great potential of nanometer-sized (Ti, Mo)C carbide. *J. Mater. Res.* **2016**, *31*, 1254–1263. [CrossRef]
17. Kim, Y.W.; Song, S.W.; Seo, S.J. Development of Ti and Mo micro-alloyed hot-rolled high strength sheet steel by controlling thermomechanical controlled processing schedule. *Mater. Sci. Eng. A* **2013**, *565*, 430–438. [CrossRef]
18. Seol, J.B.; Na, S.H.; Gault, B. Core-shell nanoparticles arrays double the strength of steel. *Sci. Rep.* **2017**, *7*, 42547. [CrossRef]
19. Wang, Z.Q.; Zhang, H.; Guo, C.H. Evolution of (Ti, Mo)C particles in austenite of a Ti-Mo-bearing steel. *Mater. Des.* **2016**, *109*, 361–366. [CrossRef]
20. Wang, Z.Q.; Zhang, H.; Guo, C.H. Effect of molybdenum addition on the precipitation of carbides in the austenite matrix of titanium micro-alloyed steels. *J. Mater. Sci.* **2016**, *51*, 4996–5007. [CrossRef]
21. Peng, Z.W.; Li, L.J.; Chen, S.J. Isothermal precipitation kinetics of carbides in undercooled austenite and ferrite of a titanium microalloyed steel. *Mater. Des.* **2016**, *108*, 289–297. [CrossRef]
22. Totten, G.E. *Steel Heat Treatment: Metallurgy of Microalloyed Steels*, 2nd ed.; CRC Press: Boca Raton, FL, USA, 1997.
23. Zhao, J.W.; Jiang, Z.Y.; Kim, J.S. Effect of tungsten on continuous cooling transformation characteristics of microalloyed steel. *Mater. Des.* **2013**, *49*, 252–258. [CrossRef]
24. Zhao, J.W.; Jiang, Z.Y.; Lee, C.S. Effect of tungsten addition and heat treatment conditions on microstructure and mechanical properties of microalloyed forging steels. *Mater. Sci. Eng. A* **2013**, *562*, 144–151. [CrossRef]
25. Zhao, J.W.; Lee, T.W.; Lee, J.H. Effects of tungsten addition on the microstructure and mechanical properties of microalloyed forging steels. *Metall. Mater. Trans. A* **2013**, *44*, 3511–3523. [CrossRef]
26. Andrens, K.W. Empirical formula for calculation of some transformation temperatures. *JISI* **1965**, *203*, 721–727.

27. Chen, J.; Tang, S.; Liu, Z. Influence of molybdenum content on transformation behavior of high performance bridge steel during continuous cooling. *Mater. Des.* **2013**, *49*, 465–470. [CrossRef]
28. Kong, J.H.; Xie, C.S. Effect of molybdenum on continuous cooling bainite transformation of low-carbon microalloyed steel. *Mater. Des.* **2006**, *27*, 1169–1173. [CrossRef]
29. Yong, Q.L. *Secondary Phases in Steels*; Metallurgical Industry Press: Beijing, China, 2006.
30. Wang, B.; Fu, W.; Li, Y. Study of the phase diagram and continuous cooling transformation of 12%Cr ultra-super-critical rotor steel. *Mater. Charact.* **2008**, *59*, 1133–1136. [CrossRef]